PROCEEDINGS A

rspa.royalsocietypublishing.org

Research

Article submitted to journal

Subject Areas:
acoustics, mathematical physics

Keywords:
asymptotic analysis, Helmholtz resonator, metamaterial, high order homogenization

Author for correspondence:
Agnès Maurel
e-mail: agnes.maurel@espci.fr

Modeling resonant arrays of the Helmholtz type in the time domain

Agnès Maurel[1], Jean-Jacques Marigo[2], Jean-François Mercier[3] and Kim Pham[4]

[1]Institut Langevin, CNRS, ESPCI ParisTech, 1 rue Jussieu, 75005 Paris, France,
[2]Laboratoire de Mécanique des Solides, CNRS, Ecole Polytechnique, 91120 Palaiseau, France,
[3]Poems, CNRS, ENSTA ParisTech, INRIA, 828 Bd des Maréchaux, 91762 Palaiseau, France,
[4]IMSIA, CNRS, ENSTA ParisTech, 828 Bd des Maréchaux, 91732 Palaiseau, France,

We present a model based on two scale asymptotic analysis for resonant arrays of the Helmholtz type, with resonators open at a single extremity (standard resonators) or open at both extremities (double-sided resonators). The effective behavior of such arrays is that of a homogeneous anisotropic slab replacing the cavity region, associated with transmission, or jump, conditions for the acoustic pressure and for the normal velocity across the region of the necks. The coefficients entering in the effective wave equation are simply related to the fraction of air in the periodic cell of the array. Those entering in the jump conditions are related to near field effects in the vicinity of the necks and they encapsulate the effects of their geometry.

The problem is written in the time domain, thus allowing us to account for complex acoustic sources. Besides, this allows us to question the problem of energy conservation in the homogenized problem, which is essential for practical numerical implementations of the homogenized problem in the time-domain.

THE ROYAL SOCIETY PUBLISHING

1. Introduction

Originally studied for their musical properties [1], the Helmholtz resonators are the most classical resonators for the acoustic waves. When organized in one or two dimensional arrays, they are known to have a collective behavior which has been used for several applications, including the improvement of edifice sonority [2] or to the opposite the reduction of noises in ventilations systems or in aircraft engines [3]. With the development of metamaterials, they have been promoted to key pieces in devices as perfect absorbers efficient in the low frequency regime [4,5], or devices acting beyond the diffraction limit, as superlenses [6] or sensors [7] designed at the subwavelength scale [8,9].

Helmholtz resonators have been largely studied in acoustics using approximate modal methods [10,11], yielding a condition of the Robin type on a plane at the top of the necks, which links the acoustic pressure to the normal velocity (this condition is written in the harmonic regime). Recently, a similar condition has been obtained using a homogenization technique based on multiple scale expansions [12]. The analysis is performed for resonators with all dimensions being $O(h)$, h being the array spacing. Although the scaling of the dimensions of the Helmholtz resonator is not discussed in this reference, it has been shown in [13] for resonators of volume $O(h^3)$ that a proper scaling of the neck opening (in $O(h^2)$) has to be chosen to recover a subwavelength resonance. Owing to this scaling, the effective properties of a set of Helmholtz resonators occupying an extended three dimensional region have been derived [14,15].

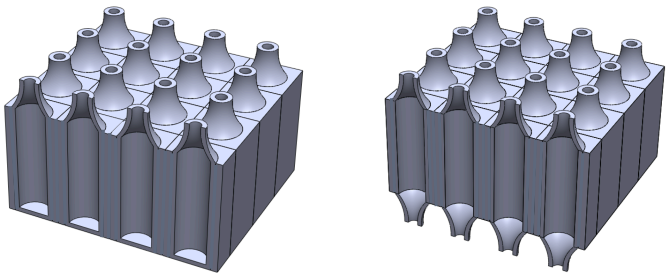

(a) (b)

Figure 1. Two dimensional arrays of resonators of the Helmholtz type (a) a standard array and (b) a two-sided array.

In the present study, we choose a scaling such that the length of the cavity is not small (it does not scale with h). In the resulting effective problem, the region of the cavities is replaced by a homogeneous and anisotropic medium while the region of the necks is replaced by jump conditions for the acoustic pressure and normal velocity, see Eqs. (2.2) in the Section 2 where our results are summarized. Our approach, presented in Section 3, is based on two-scale asymptotic analysis performed up to the second order in the small parameter h. One advantage of this approach is that it allows us to deal with arrays of standard or two-sided resonators, as shown in Fig. 1, within the same formalism. Besides, the calculations can be conducted in the time domain, since the effective parameters do not need to encapsulate the resonance as they usually do when local resonances are involved on a single row [12,16] or in an extended three-dimensional region [17]. Thus, the homogenized problems can be solved for any acoustic source, as it has been done recently for an array of rigid inclusions [18]. When such resolution in the time domain is sought, the stability of the numerical scheme requires specific properties of the equation of the energy conservation to avoid unphysical instabilities; this problem is addressed in Section

4. We report in the Appendix a discussion on the validity of our model in a simple case (two-dimensional geometry in the harmonic regime). Additional results in the harmonic regime and some minor results are collected in the Supplementary Material.

2. Summary of the main results

In this section, we summarize the main results of the study. The analysis yields an effective wave equation within the region of the cavities and jump conditions across the region of the necks, (2.2); the complete problems for the two types of arrays, standard or two -sided, simply follow.

(a) The actual and the effective problems

(i) The wave equations and the boundary conditions

In the actual problem, the linearized Euler equations have to solved in the air inside and outside the resonators, with vanishing normal velocity on the boundaries Γ of the rigid parts. The problem reads as

$$\begin{cases} \rho\dfrac{\partial \boldsymbol{u}}{\partial t} = -\boldsymbol{\nabla} p, \quad \chi\dfrac{\partial p}{\partial t} + \mathrm{div}\boldsymbol{u} = 0, \\ \\ \boldsymbol{u}\cdot\boldsymbol{n}_{|\Gamma} = 0. \end{cases} \tag{2.1}$$

In (2.1), ρ is the mass density and $\chi = (\rho c^2)^{-1}$ the isentropic compressibility of the fluid (c denotes the speed of sound in air). We shall establish that the effective problem reads as

$$\begin{cases} \rho\dfrac{\partial \boldsymbol{u}}{\partial t} = -\boldsymbol{\nabla} p, \quad \chi\dfrac{\partial p}{\partial t} + \mathrm{div}\boldsymbol{u} = 0, & \text{in } \Omega^{\pm}, \\ \\ \rho\dfrac{\partial \boldsymbol{u}}{\partial t} = -\varphi_{\mathrm{c}}\dfrac{\partial p}{\partial x_1}\boldsymbol{e}_1, \quad \chi\varphi_{\mathrm{c}}\dfrac{\partial p}{\partial t} + \mathrm{div}\boldsymbol{u} = 0, & \text{in } \Omega^{\mathrm{c}}, \\ \\ \text{with the jumps} \begin{cases} [\![p]\!] = -\rho h\mathcal{B}\,\dfrac{\partial \overline{u_1}}{\partial t}, \\ \\ [\![u_1]\!] = -h\mathcal{C}\left(\dfrac{\partial \overline{w_2}}{\partial x_2} + \dfrac{\partial \overline{w_3}}{\partial x_3}\right) - \chi e\varphi_{\mathrm{n}}\dfrac{\partial \overline{p}}{\partial t}, \end{cases} \end{cases} \tag{2.2}$$

where $\Omega^{\pm}$ refer to regions filled with air and Ω^{c} to the region replacing the region of the cavities (Figs. 2). In addition to φ_{c} the surface filling fraction of air in the cavity, we have introduced φ_{n} the volume filling fraction of air in the region of the neck; specifically, with $\mathcal{V}_{\mathrm{n}}$ the volume of air in the region of the neck (of total volume eh^2), we have $\mathcal{V}_{\mathrm{n}} = eh^2\varphi_{\mathrm{n}}$. Eventually, we defined, in Ω^{c} and $\Omega^{\pm}$, new fields w_α such that

$$\rho\frac{\partial w_\alpha}{\partial t} = -\frac{\partial p}{\partial x_\alpha}, \quad \alpha = 2, 3. \tag{2.3}$$

Note that $w_\alpha = u_\alpha$ in Ω^{+}, but it is not the case in Ω^{c} where $u_\alpha = 0$ is not linked to $\partial_{x_\alpha} p$.

Let us comment the system (2.2). The wave equation obtained in Ω^{c} is that of an anisotropic medium where the propagation is allowed along x_1 only, as expected. The waves cannot propagate across the cavity walls, thus $u_2 = u_3 = 0$. Next φ_{c} does not affect the effective sound speed being c, the same as in air (since $\partial^2 p/\partial t^2 - c^2\partial^2 p/\partial x_1^2 = 0$ from (2.2)). However, it affects the effective velocity; while $\partial_{x_1} p$ represents the velocity inside a cavity in the real problem, $\varphi_{\mathrm{c}}\partial_{x_1} p$ represents the mean flow rate in Ω^{c} in the effective problem.

Next, the jump $[\![p]\!]$ and the mean value $\overline{p}$ are defined by

$$[\![p]\!] = p^+ - p^c, \quad \overline{p} = \frac{1}{2}\left(p^+ + p^c\right), \tag{2.4}$$

with p^+ and p^c the values of p at both sides of an enlarged interface occupying the region of the necks, in Ω^+ and Ω^c respectively (the same for u_1). These jumps involve a geometrical parameter $e\varphi_n$ and the non dimensional parameters $(\mathcal{B}, \mathcal{C})$ deduced from elementary static problems, that we shall specify in the forthcoming Eqs. (3.32).

(ii) The full homogenized problems for standard and two-sided resonators

The Eqs. (2.2) have to be completed to define the full homogenized problems for standard or two-sided arrays of resonators. For standard arrays, the bottom of the cavities is rigid and the boundary condition in the effective problem is that of a vanishing normal velocity (hereafter termed rigid boundary condition), Fig. 2.(a). This has been shown in [19] for stratified media, see the Supplementary material. For double-sided arrays, the jumps in (2.2) apply at both extremities of the cavity region and obviously different neck shapes at both extremities can be accounted for by using different values of $(\mathcal{B}, \mathcal{C}, e\varphi_n)$ in the jump conditions (this is exemplified in the Supplementary material). Eventually, once the source has been defined, appropriate boundary conditions on Σ can be defined, corresponding to radiation conditions.

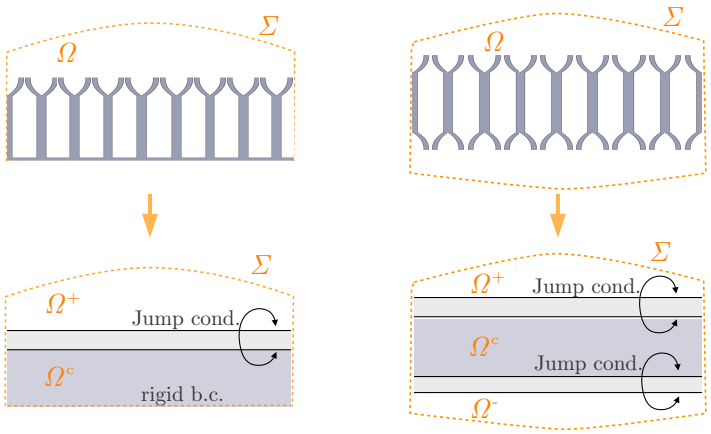

Figure 2. The actual and the effective problems for (a) a standard array and (b) a two-sided array of Helmholtz resonators with spacing h; From (2.2), Ω^e is an equivalent anisotropic medium in the cavity region, $\Omega^\pm$ is the air and jump conditions apply across the neck region/s. For (a), the rigid boundary condition applies on the bottom of the cavities.

(iii) The equation of energy conservation

In the actual problem, the equation of energy conservation reads as, from (2.1),

$$\begin{cases} \dfrac{d}{dt}\mathcal{E} + \displaystyle\int_\Sigma dS\, \boldsymbol{\Pi}.\boldsymbol{n} = 0, \\ \text{with } \mathcal{E} = \dfrac{1}{2}\displaystyle\int_\Omega dV\, \left[\rho|\boldsymbol{u}|^2 + \chi p^2\right], \quad \boldsymbol{\Pi} = p\boldsymbol{u}, \end{cases}$$

the acoustic energy and the Poynting vector respectively; the above equation holds in any bounded domain Ω (with $\partial\Omega = \Gamma \cup \Sigma$). It is useful to inspect the equation of energy conservation in the effective problem to check that the energy is positive definite. In a region Ω (with now $\partial\Omega$

including the boundaries of the enlarged interface), we shall establish from (2.2) that the equation of energy conservation reads as

$$\begin{cases} \dfrac{d}{dt}\mathcal{E} + \dfrac{d}{dt}\mathcal{E}_{\rm n} + \displaystyle\int_{\Sigma} dS\, \boldsymbol{\Pi}.\boldsymbol{n} = 0, \\ \mathcal{E}_{\rm n} = \dfrac{1}{2}\displaystyle\int \mathrm{d}\boldsymbol{x}' \ \left[\rho\, h\mathcal{B}\,\overline{u_1}^2 + \chi\, e\varphi_{\rm n}\,\overline{p}^2 + \rho h\mathcal{C}\left(\overline{w_2}^2 + \overline{w_3}^2\right)\right], \end{cases} \tag{2.5}$$

where $\mathcal{E}$ is the acoustic energy in $\Omega^{\rm c} \cup \Omega^{\pm}$ and $\mathcal{E}_{\rm n}$ is the energy supported by the interface. We shall see that $\mathcal{B}$ and $\mathcal{C}$ are positive which allows us to identify a positive definite interface energy, see [20–22]. Loosely speaking, this ensures that, in the absence of fluxes though Σ, the total energy $\mathcal{E} + \mathcal{E}_{\rm n}$ is conserved in time, without possible time variations of $\mathcal{E}$ compensated by opposite time variations of $\mathcal{E}_{\rm n}$ which would foster numerical (and unphysical) instabilities.

3. Up to second order homogenization

(a) The scaling - comments on the limit problem

(i) Scaling of the resonator

From now on and without loss of generality, we shall assume that

$$k = O(1), \quad h = \varepsilon \ll 1,$$

with k the maximum wavenumber imposed by the source. Next, we consider that all the dimensions are small except the length d of the cavity. Specifically, the scalings are (i) for the cavity, a length $d = O(1)$ and a filling fraction $\varphi_{\rm c} = O(1)$, and (ii) for the neck $e = O(\varepsilon)$, $\mathcal{S}_{\rm n} = O(\varepsilon)$ in two dimensions and $\mathcal{S}_{\rm n} = O(\varepsilon^2)$ in three dimensions.

It is worth noting that our scaling does not fulfill the traditional criterion of subwavelength resonance with respect to the length d of the cavity, but conducting the homogenization up to the second order allows us to describe the shift in the resonance toward lower frequencies; this will be commented below. Incidentally, it can be noticed that practical realizations of metasurfaces involving Helmholtz resonators have in general subwavelength neck and array spacing but not necessarily a subwavelength cavity length, see for instance in [5,23], where all dimensions h_n of the neck are typically such that $kh_n \sim 0.05$ but the cavity has a length d with $kd \sim 1$.

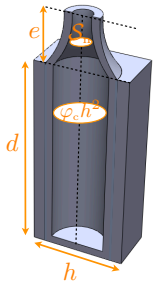

Figure 3. Dimensions of the Helmholtz resonator, with $(\mathcal{S}_{\rm n}, e)$ the cross-sectional area and the length of the neck and $\mathcal{V}_{\rm c} = \varphi_{\rm c} h^2 d$ the volume of the cavity.

(ii) The limit problem of a slot resonator

Our system (2.2) is not classical because the small parameter h is still present in the homogenized problem. In its classical form, the homogenization is performed at the first order providing a limit

problem in which the small parameter h has disappeared. In the case of Helmholtz resonators, previous studies considered that all the dimensions of the resonator scale with ε^n, $n>0$ [12,15]. These approaches allow to encapsulate the resonance at the dominant order but they have one drawback: the limit problem refers to the resonances of a close resonator thus it refers to perfect resonances. As such, the leakage, or radiative damping, of the open resonator is missing, resulting in effective parameters diverging at the resonance frequencies (note that this drawback cannot be always avoided, for instance when the resonators pave the whole space). Incidentally, as a consequence, they cannot be written in the time domain since the effective parameters depend on the frequency, by construction.

We avoid this drawback using a different scaling (whence a different limit problem) and conducting the asymptotic analysis up to the second order. Our scaling produces a limit problem in which the necks have disappeared, but not the cavities. Thus, it corresponds to a slot resonator with a quarter wavelength resonance of finite amplitude, $h=e=0$ in (2.2). Conducting the asymptotic analysis up to the order 2 allows us to recover the effect of the necks as a boundary layer correction, and to describe the shift in the resonance frequency from the quarter wavelength resonance toward lower frequencies (a shift which is dictated by h); for a discussion on boundary layer effect, see *e.g.* [24], chap. 9. In other words, the price to capture the leakage is to accept a dominant order in which a key ingredient of the Helmholtz resonance (the neck) is missing. It is recovered as a perturbation at the second order. This price is acceptable if the perturbation can be increased without affecting much the validity of the effective model, but the robustness of the model cannot be anticipated *a priori*. We collect in the Appendix A and in the Supplementary Material results in the harmonic regime which suggest that the effective model is able to describe a large range of behaviors, from the slot to the Helmholtz resonator.

(b) The asymptotic analysis

(i) The outer and inner expansions

The analysis starts with the definition of three regions where different expansions will be used. The two outer regions for $x_1>0$ and $x_1<0$ are regions where the evanescent field near the necks is negligible. There, the averaged wave equations in (2.2) are obtained and they are constructed independently in each half-spaces. The inner region refers to the region where the evanescent field is significant. Of typical extent h along x_1, it disappears in the limit problem and its effect will be captured at the second order yielding the unusual jump conditions in (2.2).

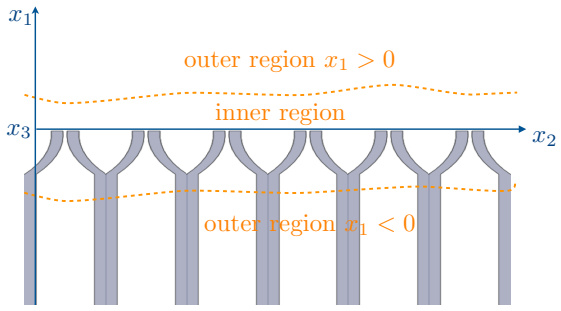

Figure 4. The outer regions, $x_1>0$ in the air, $x_1<0$ in the cavity region and the inner region containing the vicinity of the necks.

The expansions are thought with spatial dependences on a *macroscopic* coordinate $\boldsymbol{x}$ associated with the slow variations of the propagating wave (at the scale $1/k$) and a *microscopic* coordinate

$\boldsymbol{y}$, associated with the rapid variations of the evanescent field (at the scale h), with

$$\boldsymbol{y} \equiv \boldsymbol{x}/\varepsilon,$$

(remember that $h=\varepsilon$ and $k=1$), with $\boldsymbol{x}=(x_1,x_2,x_3)$ and $\boldsymbol{y}=(y_1,y_2,y_3)$. In each region, we keep the coordinates which are relevant to describe the variations of the field (this will be commented latter on). Specifically, we assume that $(p,\boldsymbol{u})$ can be expanded as

$$\left\{\begin{array}{ll} \text{outer region } x_1>0, & p=p^0(\boldsymbol{x},t)+\varepsilon p^1(\boldsymbol{x},t)+\cdots, \\ & \boldsymbol{u}=\boldsymbol{u}^0(\boldsymbol{x},t)+\varepsilon \boldsymbol{u}^1(\boldsymbol{x},t)+\cdots, \\ \text{outer region } x_1<0, & p=p^0(\boldsymbol{x},\boldsymbol{y}',t)+\varepsilon p^1(\boldsymbol{x},\boldsymbol{y}',t)+\cdots, \\ & \boldsymbol{u}=\boldsymbol{u}^0(\boldsymbol{x},\boldsymbol{y}',t)+\varepsilon \boldsymbol{u}^1(\boldsymbol{x},\boldsymbol{y}',t)+\cdots, \\ \text{inner region}, & p=q^0(\boldsymbol{x}',\boldsymbol{y},t)+\varepsilon q^1(\boldsymbol{x}',\boldsymbol{y},t)+\cdots, \\ & \boldsymbol{u}=\boldsymbol{v}^0(\boldsymbol{x}',\boldsymbol{y},t)+\varepsilon \boldsymbol{v}^1(\boldsymbol{x}',\boldsymbol{y},t)+\cdots, \end{array}\right. \tag{3.1}$$

with $\boldsymbol{x}'=(x_2,x_3)$ and $\boldsymbol{y}'=(y_2,y_3)$. Usually, the terms in the expansions are periodic with respect to the coordinates $\boldsymbol{y}'\in\mathsf{Y}$, with $\mathsf{Y}=(-1/2,1/2)^2$. In the outer region $x_1<0$ and in the inner region, due to the presence of rigid parts at $y_2=\pm 1/2$ and at $y_3=\pm 1/2$, these periodic boundary conditions do not apply all along $y_1\in(-\infty,+\infty)$, and we term below connected boundaries the boundaries where the periodic condition applies.

The above expansions will be used in (2.1) with the differential operator reading as

$$\left\{\begin{array}{lll} \text{in the outer region,} & \boldsymbol{\nabla}\to\boldsymbol{\nabla}_{\boldsymbol{x}}, & x_1>0, \\ & \boldsymbol{\nabla}\to\boldsymbol{\nabla}_{\boldsymbol{x}}+\dfrac{1}{\varepsilon}\boldsymbol{\nabla}_{\boldsymbol{y}'}, & x_1<0, \\ \text{in the inner region,} & \boldsymbol{\nabla}\to\boldsymbol{\nabla}_{\boldsymbol{x}'}+\dfrac{1}{\varepsilon}\boldsymbol{\nabla}_{\boldsymbol{y}}, & \end{array}\right. \tag{3.2}$$

where $\boldsymbol{\nabla}_{\boldsymbol{x}}$ ($\boldsymbol{\nabla}_{\boldsymbol{x}'}$) means gradient *w.r.t.* $\boldsymbol{x}$ ($\boldsymbol{x}'$) and $\boldsymbol{\nabla}_{\boldsymbol{y}}$ ($\boldsymbol{\nabla}_{\boldsymbol{y}'}$) means gradient *w.r.t.* $\boldsymbol{y}$ ($\boldsymbol{y}'$).

(ii) The boundary conditions and the matching conditions

From a unique problem, we have built three problems and we have to specify the boundary conditions which apply for each one to ensure that they are well-posed. For the inner terms,

$$\text{rigid b.c.} \quad \boldsymbol{v}^i\cdot\boldsymbol{n}=0, \quad ,i=0,1\cdots, \tag{3.3}$$

apply on the rigid parts but the conditions at infinity are unknown *a priori*. Reversely, the outer terms satisfy the radiation condition (once defined) and for $x_1<0$ they satisfy the rigid boundary condition on the walls of the cavity; however, the boundary conditions at $x_1=0^{\pm}$ are missing. These missing conditions for the inner and outer terms are provided simultaneously by so-called matching conditions which tell us that the inner and the outer expansions have to match in an intermediate regions where $x_1\to 0^{\pm}$. They are found rewriting the outer expansions with x_1 replaced by εy_1 and re-expanding in ε. We get at leading order

$$\left\{\begin{array}{ll} p^0(0^-,\boldsymbol{x}',\boldsymbol{y}',t)=\lim\limits_{y_1\to-\infty} q^0(\boldsymbol{x}',\boldsymbol{y},t), & \boldsymbol{u}^0(0^-,\boldsymbol{x}',\boldsymbol{y}',t)=\lim\limits_{y_1\to-\infty} \boldsymbol{v}^0(\boldsymbol{x}',\boldsymbol{y},t), \\ p^0(0^+,\boldsymbol{x}',t)=\lim\limits_{y_1\to+\infty} q^0(\boldsymbol{x}',\boldsymbol{y},t), & \boldsymbol{u}^0(0^+,\boldsymbol{x}',t)=\lim\limits_{y_1\to+\infty} \boldsymbol{v}^0(\boldsymbol{x}',\boldsymbol{y},t), \end{array}\right. \tag{3.4}$$

and at order ε

$$\begin{cases} p^1(0^-,\boldsymbol{x}',\boldsymbol{y}',t) = \lim\limits_{y_1\to-\infty}\left[q^1(\boldsymbol{x}',\boldsymbol{y},t) - y_1\dfrac{\partial p^0}{\partial x_1}(0^-,\boldsymbol{x}',\boldsymbol{y}',t)\right], \\ \boldsymbol{u}^1(0^-,\boldsymbol{x}',\boldsymbol{y}',t) = \lim\limits_{y_1\to-\infty}\left[\boldsymbol{v}^1(\boldsymbol{x}',\boldsymbol{y},t) - y_1\dfrac{\partial \boldsymbol{u}^0}{\partial x_1}(0^-,\boldsymbol{x}',\boldsymbol{y}',t)\right], \\ p^1(0^+,\boldsymbol{x}',t) = \lim\limits_{y_1\to+\infty}\left[q^1(\boldsymbol{x}',\boldsymbol{y},t) - y_1\dfrac{\partial p^0}{\partial x_1}(0^+,\boldsymbol{x}',t)\right], \\ \boldsymbol{u}^1(0^+,\boldsymbol{x}',t) = \lim\limits_{y_1\to+\infty}\left[\boldsymbol{v}^1(\boldsymbol{x}',\boldsymbol{y},t) - y_1\dfrac{\partial \boldsymbol{u}^0}{\partial x_1}(0^+,\boldsymbol{x}',t)\right]. \end{cases} \tag{3.5}$$

Such matching conditions have been used for different problems involving boundary layer effects at the boundary of a finite size structure [19,21] or through a thin array [20,25–27].

(c) The homogenized wave equation

The homogenized wave equation is sought for $x_1<0$ only. For $x_1>0$, from (2.1) along with (3.1) and (3.2), it simply reads as

$$\rho\frac{\partial \boldsymbol{u}^n}{\partial t} = -\boldsymbol{\nabla}_{\boldsymbol{x}} p^n, \quad \chi\frac{\partial p^n}{\partial t} + \operatorname{div}_{\boldsymbol{x}}\boldsymbol{u}^n = 0, \quad (n=0,1), \quad \text{for } x_1>0, \tag{3.6}$$

being the same at each order.

In the outer region $x_1<0$, the expansions (3.1) involve terms $p^n(\boldsymbol{x},\boldsymbol{y}',t)$, the same for $\boldsymbol{u}^n$ and we shall now comment their spatial dependence. The coordinate $\boldsymbol{x}$ gives the macroscopic position in the array of the cavities. Once the value of $\boldsymbol{x}$ has fixed a given cavity, $\boldsymbol{y}'$ accounts for small (microscopic) displacements inside the cavity; the cavities being invariant along x_1, only $\boldsymbol{y}'=(y_2,y_3)$ is needed to describe these displacements.

Now, there is a particularity due to the presence of rigid parts in the unit cell Y in the $\boldsymbol{y}'$ coordinate (Fig. 5). The Eqs. (2.1) apply in the air only, which occupies a subdomain Y_a of Y. The velocity can be extended by zero in $\mathsf{Y}\backslash\mathsf{Y}_\mathrm{a}$, which is physical and ensures the continuity of $\boldsymbol{u}.\boldsymbol{n}$ on $\partial\mathsf{Y}_\mathrm{a}$; to the opposite, the pressure cannot be defined in the rigid parts, except if we consider a specific limit problem as in [19,28]. In the following, we shall proceed differently than in [19,28], by allowing the velocity to be defined in Y but keeping the pressure defined in Y_a only. This difference in the treatment of velocity/pressure is related to the notion of extensive/intensive quantities, being respectively the flow rate and the pressure. Extending the velocity by zero in the rigid parts ensures that the flow rate in the cavities equals the flow rate in the homogenized structure. We could think to work directly in terms of flow rate/pressure, thus avoiding the extension, but the flow rate is not defined locally.

In the following, we shall establish the equations satisfied by the mean fields $(p^\mathrm{e}(\boldsymbol{x},t),\boldsymbol{u}^\mathrm{e}(\boldsymbol{x},t))$ defined by

$$p^\mathrm{e} \equiv \langle p^0\rangle + \varepsilon\langle p^1\rangle, \quad \boldsymbol{u}^\mathrm{e} \equiv \langle \boldsymbol{u}^0\rangle + \varepsilon\langle \boldsymbol{u}^1\rangle, \tag{3.7}$$

where e stands for "effective". According to what has been said above, we define the average over $\boldsymbol{y}'\in\mathsf{Y}_\mathrm{a}$ of the acoustic pressure

$$\langle p^n\rangle(\boldsymbol{x},t) \equiv \frac{1}{\varphi_\mathrm{c}}\int_{\mathsf{Y}_\mathrm{a}} \mathrm{d}\boldsymbol{y}'\, p^n(\boldsymbol{x},\boldsymbol{y}',t), \tag{3.8}$$

and the average over $\boldsymbol{y}'\in\mathsf{Y}$ of the acoustic velocity

$$\langle \boldsymbol{u}^n\rangle(\boldsymbol{x},t) \equiv \int_{\mathsf{Y}} \mathrm{d}\boldsymbol{y}'\, \boldsymbol{u}^n(\boldsymbol{x},\boldsymbol{y}',t), \tag{3.9}$$

with a vanishing velocity in $\mathsf{Y}\backslash\mathsf{Y}_\mathrm{a}$. Note that by construction, we have

$$\int_{\mathsf{Y}_\mathrm{a}} \mathrm{d}\boldsymbol{y}'\, \boldsymbol{u}^n(\boldsymbol{x},\boldsymbol{y}',t) = \langle \boldsymbol{u}^n\rangle(\boldsymbol{x},t), \quad \int_{\mathsf{Y}_\mathrm{a}} \mathrm{d}\boldsymbol{y}'\, p^n(\boldsymbol{x},\boldsymbol{y}',t) = \varphi_\mathrm{c}\, \langle p^n\rangle(\boldsymbol{x},t). \tag{3.10}$$

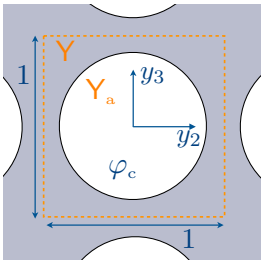

Figure 5. Unit cell in the outer region $x_1 < 0$ in $\boldsymbol{y}' = (y_2, y_3)$ coordinate.The pressure is defined in Y_a and the velocity is defined Y, being extended by $\mathbf{0}$ in $\mathsf{Y}\backslash\mathsf{Y}_\mathrm{a}$. The surface of Y in dimensionless coordinates $\boldsymbol{y}'$ equals unity, and the surface of Y_a equals φ_c.

(i) The homogenized wave equation in $x_1 < 0$ at first order

From (2.1), along with (3.1) and (3.2), we get at leading order $1/\varepsilon$ that $\boldsymbol{\nabla}_{\boldsymbol{y}'} p^0 = 0$, from which p^0 does not depend on $\boldsymbol{y}'$ and

$$p^0(\boldsymbol{x},t) = \langle p^0\rangle(\boldsymbol{x},t). \tag{3.11}$$

For simplicity, we keep the notation $p^0(\boldsymbol{x},t)$ in the following. We have also $\mathrm{div}_{\boldsymbol{y}'}\boldsymbol{u}^0 = 0$ that we shall use together with the first equation of (2.1) at the order ε^0, namely

$$\rho \frac{\partial \boldsymbol{u}^0}{\partial t}(\boldsymbol{x},\boldsymbol{y}',t) = -\left[\boldsymbol{\nabla}_{\boldsymbol{x}} p^0(\boldsymbol{x},t) + \boldsymbol{\nabla}_{\boldsymbol{y}'} p^1(\boldsymbol{x},\boldsymbol{y}',t)\right]. \tag{3.12}$$

This allows us to define the problem on p^1 which reads as

$$\begin{cases} \Delta_{\boldsymbol{y}'} p^1 = 0, \\ \left[\boldsymbol{\nabla}_{\boldsymbol{x}'} p^0(\boldsymbol{x},t) + \boldsymbol{\nabla}_{\boldsymbol{y}'} p^1(\boldsymbol{x},\boldsymbol{y}',t)\right]\cdot \boldsymbol{n}_{|\partial\mathsf{Y}_\mathrm{a}} = 0, \end{cases} \tag{3.13}$$

where we have used that $\boldsymbol{e}_1 \cdot \boldsymbol{n} = 0$. The above system has an explicit solution

$$p^1(\boldsymbol{x},\boldsymbol{y}',t) = -y_\alpha \frac{\partial p^0}{\partial x_\alpha}(\boldsymbol{x},t) + \langle p^1\rangle(\boldsymbol{x},t), \tag{3.14}$$

with $\alpha = 2,3$ (and repeated indices means summation) and with the convention for the origin such that $\langle y_\alpha\rangle = 0$. Using (3.14) in (3.12) shows that $\boldsymbol{u}^0$ does not depend on $\boldsymbol{y}'$ in Y_a, with

$$\rho \frac{\partial \boldsymbol{u}^0}{\partial t}(\boldsymbol{x},t) + \frac{\partial p^0}{\partial x_1}(\boldsymbol{x},t)\boldsymbol{e}_1 = 0, \quad \text{in } \mathsf{Y}_\mathrm{a}. \tag{3.15}$$

It is worth noting that $\boldsymbol{u}^0$ does not depend on $\boldsymbol{y}'$ in Y_a but it depends on $\boldsymbol{y}'$ in Y, with a single component along $\boldsymbol{e}_1$ being piecewise constant in Y. Finally, $\boldsymbol{u}^0$ being along $\boldsymbol{e}_1$, the continuity of $\boldsymbol{u}^0 \cdot \boldsymbol{n}$ is ensured since $u_2^0 = u_3^0 = 0$ in Y. It is now sufficient to integrate (3.15) over Y_a, with (3.10),

to get the first equation of the homogenized problem

$$\rho\frac{\partial\langle \boldsymbol{u}^0\rangle}{\partial t}(\boldsymbol{x},t)+\varphi_c\frac{\partial p^0}{\partial x_1}(\boldsymbol{x},t)\boldsymbol{e}_1=0. \tag{3.16}$$

Now, we use the second equation in (2.1) at the order ε^0

$$\chi\frac{\partial p^0}{\partial t}(\boldsymbol{x},t)+\mathrm{div}_{\boldsymbol{y}'}\boldsymbol{u}^1(\boldsymbol{x},\boldsymbol{y}',t)+\mathrm{div}_{\boldsymbol{x}}\boldsymbol{u}^0(\boldsymbol{x},\boldsymbol{y}',t)=0,\quad \text{in } \mathsf{Y}_a. \tag{3.17}$$

Integrating (3.17) over Y_a and accounting for $\boldsymbol{u}^1\cdot\boldsymbol{n}=0$ on $\partial\mathsf{Y}_a$ along with (3.10), we get

$$\chi\varphi_c\frac{\partial p^0}{\partial t}(\boldsymbol{x},t)+\mathrm{div}_{\boldsymbol{x}}\langle \boldsymbol{u}^0\rangle(\boldsymbol{x},t)=0. \tag{3.18}$$

The Eqs. (3.16) and (3.18) constitute the leading order problem in the outer region $x_1<0$.

(ii) The homogenized wave equation in $x_1<0$ at second order

The second order starts the relation

$$\mathrm{div}_{\boldsymbol{y}'}\boldsymbol{u}^1=0,\quad \text{in } \mathsf{Y}_a,$$

from (3.17)-(3.18) and $u^0(\boldsymbol{x},t)=\langle u^0\rangle(\boldsymbol{x},t)/\varphi_c$ in Y_a. Next, the first equation in (2.1) at the order ε reads $\rho\partial_t\boldsymbol{u}^1=-(\boldsymbol{\nabla}_{\boldsymbol{x}}p^1+\boldsymbol{\nabla}_{\boldsymbol{y}'}p^2)$, and with p^1 known from (3.14), we get

$$\rho\frac{\partial\boldsymbol{u}^1}{\partial t}=y_\alpha\frac{\partial}{\partial x_\alpha}\boldsymbol{\nabla}_{\boldsymbol{x}}p^0(\boldsymbol{x},t)-\boldsymbol{\nabla}_{\boldsymbol{x}}\langle p^1\rangle(\boldsymbol{x},t)-\boldsymbol{\nabla}_{\boldsymbol{y}'}p^2, \tag{3.19}$$

(with $\alpha=2,3$ and repeated indices means summation). This gives us the problem on p^2 which reads as

$$\begin{cases}\Delta_{\boldsymbol{y}'}p^2(\boldsymbol{x},\boldsymbol{y}',t)=\Delta_{\boldsymbol{x}'}p^0(\boldsymbol{x},t),\quad \text{in } \mathsf{Y}_a,\\ \left(\boldsymbol{\nabla}_{\boldsymbol{y}'}p^2-y_\alpha\dfrac{\partial^2p^0}{\partial x_\alpha\partial x_\beta}(\boldsymbol{x},t)\mathbf{e}_\beta+\boldsymbol{\nabla}_{\boldsymbol{x}'}\langle p^1\rangle(\boldsymbol{x},t)\right)\cdot\boldsymbol{n}_{|\partial\mathsf{Y}_a}=0,\end{cases} \tag{3.20}$$

whose solution is explicit and of the form

$$p^2(\boldsymbol{x},\boldsymbol{y}',t)=\frac{y_\alpha y_\beta}{2}\frac{\partial^2p^0}{\partial x_\alpha\partial x_\beta}(\boldsymbol{x},t)-y_\alpha\frac{\partial\langle p^1\rangle}{\partial x_\alpha}(\boldsymbol{x},t)+\hat{p}^2(\boldsymbol{x},t), \tag{3.21}$$

with $\beta=2,3$ and repeated indices means summation (note that $\hat{p}^2$ does not equal $\langle p^2\rangle$). Using (3.21) in (3.19), we get

$$\rho\frac{\partial\boldsymbol{u}^1}{\partial t}(\boldsymbol{x},\boldsymbol{y},t)=\left[y_\alpha\frac{\partial^2p^0}{\partial x_\alpha\partial x_1}(\boldsymbol{x},t)-\frac{\partial\langle p^1\rangle}{\partial x_1}(\boldsymbol{x},t)\right]\boldsymbol{e}_1. \tag{3.22}$$

At the order 1, the velocity is still along $\boldsymbol{e}_1$ as expected, but now it depends on $\boldsymbol{y}'$ in Y_a. Once integrated over Y_a, with (3.10) and using that $\langle y_\alpha\rangle=0$, we get

$$\rho\frac{\partial\langle\boldsymbol{u}^1\rangle}{\partial t}(\boldsymbol{x},t)=-\varphi_c\frac{\partial\langle p^1\rangle}{\partial x_1}(\boldsymbol{x},t)\boldsymbol{e}_1. \tag{3.23}$$

The last step consists in integrating over Y_a the second equation of (2.1) at the order ε, namely $\chi\partial_t p^1+\mathrm{div}_{\boldsymbol{y}'}\boldsymbol{u}^2+\mathrm{div}_{\boldsymbol{x}}\boldsymbol{u}^1=0$, which leaves us with

$$\chi\varphi_c\frac{\partial\langle p^1\rangle}{\partial t}(\boldsymbol{x},t)+\frac{\partial\langle u_1^1\rangle}{\partial x_1}(\boldsymbol{x},t)=0. \tag{3.24}$$

The Eqs. (3.23) and (3.24) define the problem at the order 2 in the outer region $x_1<0$.

(iii) Up to second-order homogenized wave equation

The final up to second-order homogenized wave equation is obtained gathering (3.16), (3.18) and (3.23), (3.24) and it reads, for $(p^{\mathrm{e}}, \boldsymbol{u}^{\mathrm{e}})$ defined in (3.7), as

$$\rho \frac{\partial \boldsymbol{u}^{\mathrm{e}}}{\partial t} = -\varphi_{\mathrm{c}} \frac{\partial p^{\mathrm{e}}}{\partial x_1} \boldsymbol{e}_1, \quad \chi \varphi_{\mathrm{c}} \frac{\partial p^{\mathrm{e}}}{\partial t} + \mathrm{div}_{\boldsymbol{x}} \boldsymbol{u}^{\mathrm{e}} = 0, \tag{3.25}$$

as $(p, \boldsymbol{u})$ in (2.2).

(d) The jump conditions

To the homogenized wave equation (3.25) we have to associate boundary conditions when approaching the necks, at $x_1 = 0^-$, as we have to associate boundary conditions for the outer problem in the air at $x_1 = 0^+$ (Fig. 4). We shall see that the usual continuities of the pressure and of the normal velocity are obtained at the leading order while the second order makes discontinuities of these two fields to appear.

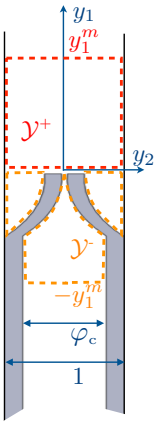

Figure 6. The three dimensional elementary cell in $\boldsymbol{y} = (y_1, y_2, y_3)$ coordinate where the inner problem is analyzed. The elementary cell is a strip, bounded in the $\boldsymbol{y}'$ plane and infinite along $y_1 \in (-\infty, +\infty)$. We shall use the integration domain $\mathcal{Y} = \mathcal{Y}^- \cup \mathcal{Y}^+$ with $y_1 \in (-y_1^m, y_1^m)$.

Let us start by commenting the form of the inner terms in (3.1) that we have written with a dependence in $\boldsymbol{y}$ and $\boldsymbol{x}'$. The coordinate $\boldsymbol{x}'$ gives the macroscopic position in the plane containing the necks. Once the value of $\boldsymbol{x}'$ has fixed a given neck, $\boldsymbol{y}$ accounts for small displacements around the neck. In particular, y_1 approaching $-\infty$ and $+\infty$ in the inner problem corresponds to x_1 approaching 0^- and 0^+ in the outer problem. Thus, the inner problem is defined in a strip infinite along y_1 with $\boldsymbol{y}'$ bounded in Y_{a} insides the cavity and bounded in $(-1/2, 1/2)^2$ in the air (Fig. 6). In the following, we shall use the integration domain $\mathcal{Y}$ of air for $y_1 \in (-y_1^m, y_1^m)$; $\mathcal{Y}^-$ and $\mathcal{Y}^+$ are the subdomains of $\mathcal{Y}$ corresponding to $y_1 < 0$ and $y_1 > 0$, respectively. Thus, in $\mathcal{Y}^+$, the inner terms are periodic with respect to $\boldsymbol{y}'$; in $\mathcal{Y}^-$, both rigid boundary condition (3.3) and periodic condition (on the connected boundaries) apply.

Let us precise a last point. We have defined in (2.4) jump conditions across the region of the necks, denoted $[\![.]\!]$. In this section, and following [20–22,27,29,30], we shall first derive jumps defined across a zero thickness interface at $x_1 = 0$, that we denote $[\![.]\!]_0$. The extension to the jumps across an enlarged version of the interface is considered in Section (d).iv and the consequence on the sign of the interface energy is discussed in Section 4.

(i) The jumps of the pressure and of the velocity at the first order

Inserting the inner expansion (3.1) in the first equation of (2.1) tells us that, at the leading order in $1/\varepsilon$, $\boldsymbol{\nabla}_{\boldsymbol{y}'} q^0 = 0$ from which

$$q^0(\boldsymbol{x}', \boldsymbol{y}, t) = q^0(\boldsymbol{x}', t) = p^0(0^{\pm}, \boldsymbol{x}', t), \quad \text{thus } \left[\!\left[p^0 \right]\!\right]_0 = 0. \tag{3.26}$$

Next, we integrate $\mathrm{div}_{\boldsymbol{y}} \boldsymbol{v}^0 = 0$ over $\mathcal{Y}$. Accounting for the boundary conditions ($\boldsymbol{v}^0 \cdot \boldsymbol{n} = 0$ on the rigid parts and $\boldsymbol{v}^0$ periodic on the connected boundaries), we get

$$\int_{\mathsf{Y}} \mathrm{d}\boldsymbol{y}'\, v_1^0(\boldsymbol{x}', y_1^m, \boldsymbol{y}', t) - \int_{\mathsf{Y}_a} \mathrm{d}\boldsymbol{y}'\, v_1^0(\boldsymbol{x}', -y_1^m, \boldsymbol{y}', t) = 0. \tag{3.27}$$

It is now sufficient to consider the limit $y_1^m \to \infty$ and the matching condition (3.4) to conclude that

$$\int_{\mathsf{Y}} \mathrm{d}\boldsymbol{y}'\, u_1^0(0^+, \boldsymbol{x}', t) = \int_{\mathsf{Y}_a} \mathrm{d}\boldsymbol{y}'\, u_1^0(0^-, \boldsymbol{x}', \boldsymbol{y}', t), \tag{3.28}$$

whence, from (3.10),

$$\left[\!\left[\langle u_1^0 \rangle \right]\!\right]_0 = 0. \tag{3.29}$$

At the leading order, we obtain the usual continuities of the pressure and of the normal velocity, this latter being in fact a continuity of the fluxes. In [19], it has been shown for a slot resonator that these continuity conditions are already satisfactory and going up to the second order improves the range of validity of the effective model. In the present case, we expect that accounting for the boundary layer effects would allows us to move from the slot resonance toward the Helmholtz resonance (see Appendix A).

(ii) The jump of the pressure at the second order

To begin with, we shall define the problem satisfied by $(q^1, \boldsymbol{v}^0)$, specifically

$$\begin{cases} \mathrm{div}_{\boldsymbol{y}} \boldsymbol{v}^0 = 0, \quad \rho \dfrac{\partial \boldsymbol{v}^0}{\partial t} = -\boldsymbol{\nabla}_{\boldsymbol{x}'} p^0(0, \boldsymbol{x}', t) - \boldsymbol{\nabla}_{\boldsymbol{y}} q^1, \quad \boldsymbol{v}^0 \cdot \boldsymbol{n}_{|\Gamma} = 0, \\ \lim\limits_{y_1 \to -\infty} \dfrac{\partial \boldsymbol{v}^0}{\partial t} = \dfrac{1}{\varphi_{\mathrm{c}}} \dfrac{\partial \langle u_1^0 \rangle}{\partial t}(0, \boldsymbol{x}', t)\, \boldsymbol{e}_1. \\ \lim\limits_{y_1 \to +\infty} \dfrac{\partial \boldsymbol{v}^0}{\partial t} = \dfrac{\partial \langle u_1^0 \rangle}{\partial t}(0, \boldsymbol{x}', t)\, \boldsymbol{e}_1 - \dfrac{1}{\rho} \boldsymbol{\nabla}_{\boldsymbol{x}'} p^0(0, \boldsymbol{x}', t). \end{cases} \tag{3.30}$$

To get the limits when $y_1 \to \pm\infty$, we used the time derivative versions of the matching conditions (3.4) on $\boldsymbol{v}^0$. Next, for $y_1 \to -\infty$, we know from (3.15) that $u_\alpha^0 = 0$, $\alpha = 2, 3$ and we have $\langle u_1^0 \rangle = \varphi_{\mathrm{c}} u_1^0$ since u_1^0 does not depend on $\boldsymbol{y}'$. The limit $y_1 \to +\infty$ has been obtained from (3.6) with $\rho \partial_t \boldsymbol{u}^0 = -\boldsymbol{\nabla}_{\boldsymbol{x}} p^0$ and using that $\langle u_1^0 \rangle = u_1^0$. We have written the problem (3.30) in terms of the three independent fields $\partial_t \langle u_1^0 \rangle$ and $\partial_{x_\alpha} p^0$, $\alpha = 2, 3$. Thus, by linearity, we can define

$$q^1(\boldsymbol{x}', \boldsymbol{y}, t) = -\rho \frac{\partial \langle u_1^0 \rangle}{\partial t}(0, \boldsymbol{x}', t) Q_1(\boldsymbol{y}) + \frac{\partial p^0}{\partial x_\alpha}(0, \boldsymbol{x}', t)\, (Q_\alpha(\boldsymbol{y}) - y_\alpha) + \langle q^1 \rangle(\boldsymbol{x}', t), \tag{3.31}$$

where Q_1 and Q_α are functions of $\boldsymbol{y}$ only and they satisfy the so-called elementary problems

$$\begin{cases} \Delta Q_1 = 0, \quad \partial_n Q_{1|\Gamma} = 0, \quad \lim\limits_{y_1 \to -\infty} \boldsymbol{\nabla} Q_1 = \dfrac{\boldsymbol{e}_1}{\varphi_{\mathrm{c}}}, \quad \lim\limits_{y_1 \to +\infty} \boldsymbol{\nabla} Q_1 = \boldsymbol{e}_1, \\ \Delta Q_\alpha = 0, \quad \partial_n Q_{\alpha|\Gamma} = 0, \quad \lim\limits_{y_1 \to -\infty} \boldsymbol{\nabla} Q_\alpha = \boldsymbol{0}, \quad \lim\limits_{y_1 \to +\infty} \boldsymbol{\nabla} Q_\alpha = \boldsymbol{e}_\alpha, \end{cases} \tag{3.32}$$

and Q_1, $(Q_\alpha - y_\alpha)$ are periodic with respect to y_2 and y_3 in the connected regions. The above problems are classical problems of potential flows, as illustrated Figure 7.

In (3.31), we introduced $\langle q^1 \rangle(\boldsymbol{x}', t)$ since $q^1(\boldsymbol{x}', \boldsymbol{y}, t)$ is defined in (3.30) up to a function independent of $\boldsymbol{y}$; doing so, we assume implicitly that $\langle Q_1 \rangle = \langle Q_\alpha \rangle = 0$ (Q_1 and Q_α are defined up to a constant and the constant is determined by the condition of zero average). When $y_1 \to \pm\infty$,

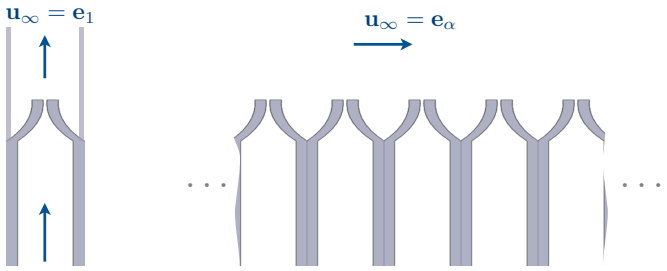

(a) (b)

Figure 7. Elementary problems (3.32) corresponding to potential flow problems, (a) Q_1 is the velocity potential for a perfect fluid flowing in a duct along the centerline and (b) Q_α is the velocity potential for a perfect fluid flowing along $\mathbf{e}_\alpha$ over an array.

the functions Q_1 and Q_α have a linear behavior with respect to y_1 and y_α respectively. Specifically, their limits read as

$$\begin{cases} \text{when } y_1 \to -\infty, \quad Q_1 \sim \dfrac{y_1}{\varphi_c} + \mathcal{B}_1^-, \quad Q_\alpha \sim 0, \\ \text{when } y_1 \to +\infty, \quad Q_1 \sim y_1 + \mathcal{B}_1^+, \quad Q_\alpha \sim y_\alpha. \end{cases} \tag{3.33}$$

We have used that Q_α, $\alpha = 2, 3$, is odd with respect to y_α (up to contant), and to satisfy $\langle Q_\alpha \rangle = 0$, the constant has to be 0. This is not the same for Q_1 which is axisymmetric in the (y_2, y_3) plane which allows the constants to be different at $y_1 \to \pm\infty$. The jump in p^1 directly follows from the matching conditions on the pressure in (3.5), along with (3.31) and (3.33), leading to

$$\begin{cases} p^1(0^-, \boldsymbol{x}', \boldsymbol{y}', t) = -\rho \mathcal{B}_1^- \dfrac{\partial \langle u_1^0 \rangle}{\partial t}(0, \boldsymbol{x}', t) - \dfrac{\partial p^0}{\partial x_\alpha}(0, \boldsymbol{x}', t) y_\alpha + \langle q^1 \rangle (\boldsymbol{x}', t), \\ p^1(0^+, \boldsymbol{x}', t) = -\rho \mathcal{B}_1^+ \dfrac{\partial \langle u_1^0 \rangle}{\partial t}(0, \boldsymbol{x}', t) + \langle q^1 \rangle (\boldsymbol{x}', t), \end{cases} \tag{3.34}$$

We have used that (i) $\partial_{x_1} p^0(0^-, \boldsymbol{x}', t) = -\rho \partial_t \langle u_1^0 \rangle (0, \boldsymbol{x}', t)/\varphi_c$, from (3.15), for the former limit and (ii) $\partial_{x_1} p^0(0^+, \boldsymbol{x}', t) = -\rho \partial_t \langle u_1^0 \rangle (0, \boldsymbol{x}', t)$, from (3.6), for the latter limit. Eventually, taking the average of $p^1(0^-, \boldsymbol{x}', \boldsymbol{y}', t)$ over Y_a and using that $\langle y_\alpha \rangle = 0$ leave us with

$$\left[\!\left[\langle p^1 \rangle \right]\!\right]_0 = -\rho \mathcal{B}_1 \frac{\partial \langle u_1^0 \rangle}{\partial t}(0, \boldsymbol{x}', t), \tag{3.35}$$

where

$$\mathcal{B}_1 = \mathcal{B}_1^+ - \mathcal{B}_1^-. \tag{3.36}$$

(iii) The jump of the velocity at the second order

We now have to determine the jump in u_1^1 and this is a little more involved. We start with the relation $\chi \partial_t q^0 + \mathrm{div}_{\boldsymbol{y}} \boldsymbol{v}^1 + \mathrm{div}_{\boldsymbol{x}'} \boldsymbol{v}^0 = 0$. We use that $q^0 = p^0(0, \boldsymbol{x}', t)$ from (3.26), and integrate over $\mathcal{Y}$ the time derivative version of this relation, namely

$$\frac{\partial}{\partial t} \int_{\mathcal{Y}} \mathrm{d}\boldsymbol{y} \left[\chi \frac{\partial p^0}{\partial t}(0, \boldsymbol{x}', t) + \mathrm{div}_{\boldsymbol{y}} \boldsymbol{v}^1 + \mathrm{div}_{\boldsymbol{x}'} \boldsymbol{v}^0 \right] = 0. \tag{3.37}$$

This integral involves 3 terms that we shall consider now.

• The first integral is trivial and involves only the volume of $\mathcal{Y}$, specifically

$$\frac{\partial}{\partial t}\int_{\mathcal{Y}} \mathrm{d}\boldsymbol{y}\, \chi \frac{\partial p^0}{\partial t}(0,\boldsymbol{x}',t) = \chi \frac{\partial^2 p^0}{\partial t^2}(0,\boldsymbol{x}',t)\,\left[y_1^m + \varphi_{\mathrm{c}}\left(y_1^m - \frac{e}{h}\right) + \varphi_{\mathrm{n}}\frac{e}{h}\right], \tag{3.38}$$

(φ_{c}, φ_{n} are the filling fraction of air in the cavity and in the region of the neck).

• The second integral reads as

$$\frac{\partial}{\partial t}\int_{\mathcal{Y}} \mathrm{d}\boldsymbol{y}\, \mathrm{div}_{\boldsymbol{y}}\boldsymbol{v}^1 = \frac{\partial}{\partial t}\left[\int_{\mathrm{Y}} \mathrm{d}\boldsymbol{y}'\, v_1^1(\boldsymbol{x}',y_1^m,\boldsymbol{y}',t) - \int_{\mathrm{Y_a}} \mathrm{d}\boldsymbol{y}'\, v_1^1(\boldsymbol{x}',-y_1^m,\boldsymbol{y}',t)\right]. \tag{3.39}$$

Passing to the limit when $y_1^m \to \infty$, along with the matching condition in (3.5), we get

$$\lim_{y_1^m\to+\infty}\frac{\partial}{\partial t}\int_{\mathcal{Y}} \mathrm{d}\boldsymbol{y}\, \mathrm{div}_{\boldsymbol{y}}\boldsymbol{v}^1 = \frac{\partial}{\partial t}\left[\!\!\left[\langle u_1^1\rangle\right]\!\!\right]_0 + \lim_{y_1^m\to+\infty} y_1^m \frac{\partial}{\partial t}\left(\frac{\partial\langle u_1^0\rangle}{\partial x_1}(0^-,\boldsymbol{x}',t) + \frac{\partial\langle u_1^0\rangle}{\partial x_1}(0^+,\boldsymbol{x}',t)\right). \tag{3.40}$$

• The third integral is $\partial_t \int \mathrm{div}_{\boldsymbol{x}'}\boldsymbol{v}^0$ involves typically $\partial_{x_2}\partial_t v_2^0$ and this term is given in (3.30) with q^1 in (3.31), whence

$$\frac{\partial}{\partial t}\frac{\partial v_2^0}{\partial x_2} = -\frac{1}{\rho}\frac{\partial^2 p^0}{\partial x_2^2}(0,\boldsymbol{x}') + \frac{\partial}{\partial t}\frac{\partial\langle u_1^0\rangle}{\partial x_2}(0,\boldsymbol{x}')\frac{\partial Q_1}{\partial y_2}(\boldsymbol{y}) - \frac{1}{\rho}\frac{\partial^2 p^0}{\partial x_\alpha \partial x_2}(0,\boldsymbol{x}')\left(\frac{\partial Q_\alpha}{\partial y_2}(\boldsymbol{y}) - \delta_{2\alpha}\right), \tag{3.41}$$

or equivalently

$$\frac{\partial}{\partial t}\frac{\partial v_2^0}{\partial x_2} = \frac{\partial}{\partial t}\frac{\partial\langle u_1^0\rangle}{\partial x_2}(0,\boldsymbol{x}')\frac{\partial Q_1}{\partial y_2}(\boldsymbol{y}) - \frac{1}{\rho}\frac{\partial^2 p^0}{\partial x_2\partial x_\alpha}(0,\boldsymbol{x}')\frac{\partial Q_\alpha}{\partial y_2}(\boldsymbol{y}). \tag{3.42}$$

From (3.32), the integrals over $\mathcal{Y}$ of $\partial_{y_2}Q_1$ and $\partial_{y_2}Q_3$ are bounded. Next, $\partial_{y_2}Q_2$ is integrable on $\mathcal{Y}^-$ and that $(\partial_{y_2}Q_2 - 1)$ is integrable on $\mathcal{Y}^+$. Thus, we use (3.42) when integrating over $\mathcal{Y}^-$ and (3.41) when integrating over $\mathcal{Y}^+$, and we obtain

$$\begin{cases} \dfrac{\partial}{\partial t}\displaystyle\int_{\mathcal{Y}^-} \mathrm{d}\boldsymbol{y}\, \frac{\partial v_2^0}{\partial x_2} = \frac{\partial}{\partial t}\frac{\partial\langle u_1^0\rangle}{\partial x_2}(0,\boldsymbol{x}',t)\displaystyle\int_{\mathcal{Y}^-} \mathrm{d}\boldsymbol{y}\, \frac{\partial Q_1}{\partial y_2}(\boldsymbol{y}) - \frac{1}{\rho}\frac{\partial^2 p^0}{\partial x_2\partial x_\alpha}(0,\boldsymbol{x}',t)\displaystyle\int_{\mathcal{Y}^-} \mathrm{d}\boldsymbol{y}\, \frac{\partial Q_\alpha}{\partial y_2}(\boldsymbol{y}), \\ \dfrac{\partial}{\partial t}\displaystyle\int_{\mathcal{Y}^+} \mathrm{d}\boldsymbol{y}\, \frac{\partial v_2^0}{\partial x_2} = -\frac{y_1^m}{\rho}\frac{\partial^2 p^0}{\partial x_2^2}(0,\boldsymbol{x}',t), \end{cases} \tag{3.43}$$

where we have used in $\mathcal{Y}^+$ the periodicity of Q_1, $(Q_2 - y_2)$ and Q_3. Doing the same for $\partial_t\partial_{x_3}v_3^0$, we get

$$\frac{\partial}{\partial t}\int_{\mathcal{Y}} \mathrm{div}_{\boldsymbol{x}'}\boldsymbol{v}^0 = -\frac{\mathcal{C}}{\rho}\Delta_{\boldsymbol{x}'}p^0(0,\boldsymbol{x}',t) - \frac{y_1^m}{\rho}\Delta_{\boldsymbol{x}'}p^0(0,\boldsymbol{x}',t), \tag{3.44}$$

where

$$\mathcal{C} = \int_{\mathcal{Y}^-} \mathrm{d}\boldsymbol{y}\, \frac{\partial Q_2}{\partial y_2} = \int_{\mathcal{Y}^-} \mathrm{d}\boldsymbol{y}\, \frac{\partial Q_3}{\partial y_3}. \tag{3.45}$$

In this last step, we have used that $\int_{\mathcal{Y}^-} \mathrm{d}\boldsymbol{y}\, \partial_{y_\alpha}Q_1 = 0$ and that $\int_{\mathcal{Y}^-} \mathrm{d}\boldsymbol{y}\, \partial_{y_2}Q_3 = \int_{\mathcal{Y}^-} \mathrm{d}\boldsymbol{y}\, \partial_{y_3}Q_2 = 0$ (Q_2 is even *w.r.t.* y_3 and Q_1 is even *w.r.t.* y_2 and y_3).

We now collect the terms in the 3 integrals which are linear in y_1^m. Their sum reads as

$$\begin{aligned} y_1^m \quad & \left[\frac{\partial}{\partial t}\left(\chi\varphi_{\mathrm{c}}\frac{\partial p^0}{\partial t}(0,\boldsymbol{x}',t) + \frac{\partial\langle u_1^0\rangle}{\partial x_1}(0^-,\boldsymbol{x}',t)\right)\right. \\ & \left. + \left(\chi\frac{\partial^2 p^0}{\partial t^2}(0,\boldsymbol{x}',t) + \frac{\partial}{\partial t}\frac{\partial\langle u_1^0\rangle}{\partial x_1}(0^+,\boldsymbol{x}',t) - \frac{1}{\rho}\Delta_{\boldsymbol{x}'}p^0(0,\boldsymbol{x}',t)\right)\right], \end{aligned} \tag{3.46}$$

where we have separated two contribution intentionally: the first parenthesis vanishes owing to the wave equation (3.18) in $\mathcal{Y}^-$ (along with $\langle\boldsymbol{u}^0\rangle = \langle u_1^0\rangle\boldsymbol{e}_1$ from (3.16)), and the second parenthesis vanishes owing to the wave equation (3.6) in $\mathcal{Y}^+$. Thus, and as expected, the diverging terms

vanish and we finally get

$$\frac{\partial}{\partial t}\left[\!\left[\langle u_1^1\rangle\right]\!\right]_0 = -\chi\,(\varphi_{\rm n}-\varphi_{\rm c})\,\frac{e}{h}\frac{\partial^2 p^0}{\partial t^2}(0,\boldsymbol{x}',t) + \frac{\mathcal{C}}{\rho}\Delta_{\boldsymbol{x}'}p^0(0,\boldsymbol{x}',t). \tag{3.47}$$

In order to get a jump condition in u_1^1 without time derivative, we define $w_\alpha^0(\boldsymbol{x},t)$ such as

$$\rho\frac{\partial w_\alpha^0}{\partial t} = -\frac{\partial p^0}{\partial x_\alpha}, \quad \alpha = 2,3, \tag{3.48}$$

whence

$$\left[\!\left[u_1^1\right]\!\right]_0 = -\chi\,(\varphi_{\rm n}-\varphi_{\rm c})\,\frac{e}{h}\frac{\partial p^0}{\partial t}(0,\boldsymbol{x}',t) - \mathcal{C}\,\frac{\partial w_\alpha^0}{\partial x_\alpha}(0,\boldsymbol{x}',t). \tag{3.49}$$

Obviously, in $\mathcal{Y}^+$, $u_\alpha^0 = w_\alpha^0$, but in $\mathcal{Y}^-$ this is not the case since $u_\alpha^0 = 0$ is not linked to w_α^0.

(iv) Final jump conditions across an enlarged interface

The final jump conditions will be written for $(p^{\rm e},\boldsymbol{u}^{\rm e})$ defined in (3.7). In addition, we shall consider the jumps across an enlarged interface, namely between $x_1=-e$ and $x_1=0$ (in their present forms, they are written between $x_1=0^-$ and $x_1=0^+$). It has been already discussed that the resulting problem is equivalent up to $O(\varepsilon^2)$ to the problem with a zero thickness interface. Besides, the problem involving an enlarged version of the interface is associated to a positive interface energy and this will be discussed in the present case below. Thus, we want the jumps defined as

$$[\![p^{\rm e}]\!] = p^{\rm e}(0^+,\boldsymbol{x}',t) - p^{\rm e}(-e,\boldsymbol{x}',t), \tag{3.50}$$

with $e=O(\varepsilon)$ (the jump defined above corresponds to the definition in (2.4)). We shall essentially use that

$$\begin{cases} p^0(-e,\boldsymbol{x}',t) = p^0(0^-,\boldsymbol{x}',t) - e\dfrac{\partial p^0}{\partial x_1}(-e,\boldsymbol{x}',t) + O(\varepsilon^2), \\ \varepsilon\langle p^1\rangle(-e,\boldsymbol{x}',t) = \varepsilon\langle p^1\rangle(0^-,\boldsymbol{x}',t) + O(\varepsilon^2). \end{cases} \tag{3.51}$$

It follows that $[\![p^{\rm e}]\!] = e\partial_{x_1}p^0(-e,\boldsymbol{x}',t) + \varepsilon\left[\!\left[\langle p^1\rangle\right]\!\right]_0 + O(\varepsilon^2)$. With $x_1=-e<0$, we have $\partial_{x_1}p^0 = -(\rho/\varphi_{\rm c})\partial_t\langle u_1^0\rangle$ from (3.15) and we get

$$[\![p^{\rm e}]\!] = -\rho\,h\mathcal{B}\,\frac{\partial\langle u_1^0\rangle}{\partial t}(0,\boldsymbol{x}',t) + O(\varepsilon^2), \tag{3.52}$$

where we have defined

$$h\mathcal{B} = h\mathcal{B}_1 + \frac{e}{\varphi_{\rm c}}. \tag{3.53}$$

Doing the same for $[\![u_1^{\rm e}]\!] = e\partial_{x_1}u_1^0(-e,\boldsymbol{x}',t) + \varepsilon\left[\!\left[u_1^1\right]\!\right]_0 + O(\varepsilon^2)$, and using that $\partial_{x_1}u_1^0 = -\varphi_{\rm c}\chi\partial_t p^0$ from (3.18), we obtain that

$$[\![u_1^{\rm e}]\!] = \quad h\mathcal{C}\,\frac{\partial w_\alpha^0}{\partial x_\alpha}(0,\boldsymbol{x}',t) - \chi\,\varphi_{\rm n}e\frac{\partial p^0}{\partial t}(0,\boldsymbol{x}',t) + O(\varepsilon^2). \tag{3.54}$$

It is easy to see that $(p,\boldsymbol{u})$ satisfying (2.2) have the same expansions than $(p^{\rm e},\boldsymbol{u}^{\rm e})$ satisfying (3.25) with the jumps (3.52) and (3.54) up to $O(\varepsilon^2)$, thus (2.2) constitutes our final homogenized problem.

4. The energy conservation in the effective problem

In this section, we shall derive the form of the energy $\mathcal{E}_{\rm n}$ supported by the interface and show that $\mathcal{E}_{\rm n}$ is positive definite. The calculations are performed for an array of standard Helmholtz resonators, and the calculations for an array of double-sided resonator follow straightforwardly.

(a) The energy $\mathcal{E}_{\rm n}$ supported by the interface

In the homogenized problem, the equation of the energy conservation is written starting from (2.2). It is easy to see that we get

$$\left\{\begin{array}{l} \dfrac{1}{2}\dfrac{d}{dt}\mathcal{E}+\displaystyle\int_{\partial\Omega^+\cup\partial\Omega^{\rm c}} {\rm d}S\, p\boldsymbol{u}\cdot\boldsymbol{n}=0, \\ \mathcal{E}=\dfrac{1}{2}\displaystyle\int_{\Omega^{\rm c}} {\rm d}\boldsymbol{x}\,\left[\frac{\rho}{\varphi_{\rm c}}\,{u_1}^2+\chi\varphi_{\rm c}\,p^2\right]+\frac{1}{2}\int_{\Omega^+} {\rm d}\boldsymbol{x}\,\left[\rho|\boldsymbol{u}|^2+\chi\,p^2\right]. \end{array}\right. \tag{4.1}$$

The fluxes through $\partial\Omega^+\cup\partial\Omega^{\rm c}$ involve the ingoing and outgoing fluxes through Σ as in the actual problem (Fig. 2), but they involve also a flux Φ through the interface where the jump conditions apply. Specifically, we have

$$\int_{\partial\Omega^+\cup\partial\Omega^{\rm c}} {\rm d}S\, p\boldsymbol{u}\cdot\boldsymbol{n}=\Phi+\int_{\Sigma} {\rm d}S\, p\boldsymbol{u}\cdot\boldsymbol{n},\quad \text{with}\ \ \Phi=-\int {\rm d}\boldsymbol{x}'\ [\![pu_1]\!]\,, \tag{4.2}$$

where we use the convention of the x_1 axis normal to the interface and pointing from $\Omega^{\rm c}$ to Ω^+. In (2.5), we have said that $-\int {\rm d}\boldsymbol{x}'\ [\![pu_1]\!]$ can be expressed as the time derivative of an energy $\mathcal{E}_{\rm n}$, and we shall see that this is the case and besides, that $\mathcal{E}_{\rm n}\geq 0$. We start with

$$\Phi=-\int {\rm d}\boldsymbol{x}'\ [\![u_1]\!]\,\overline{p}-\int {\rm d}\boldsymbol{x}'\ \overline{u_1}\,[\![p]\!]=\frac{1}{2}\frac{d}{dt}\int {\rm d}\boldsymbol{x}'\ \left[\rho\, h\mathcal{B}\,\overline{u_1}^2+\chi\varphi_{\rm n}e\,\overline{p}^2\right]+\int {\rm d}\boldsymbol{x}'\ h\mathcal{C}\,\overline{p}\,\frac{\partial\overline{w_\alpha}}{\partial x_\alpha}. \tag{4.3}$$

It is now sufficient to use the integrations by part $\int {\rm d}\boldsymbol{x}'\,\overline{p}\,\partial_{x_\alpha}\overline{w_\alpha}=-\int {\rm d}\boldsymbol{x}'\,\overline{w_\alpha}\partial_{x_\alpha}\overline{p}+{\rm b{\cdot}t{\cdot}}$ where b·t· means boundary terms that should be considered at the extremities of the equivalent interface; they are disregarded here. From (2.3), $\int {\rm d}\boldsymbol{x}'\,\overline{p}\,\partial_{x_\alpha}\overline{w_\alpha}=\rho\int {\rm d}\boldsymbol{x}'\,\overline{w_\alpha}\partial_t\overline{w_\alpha}$. Inserting the above result with (4.2) and (4.1) gives the equation of energy conservation (2.5).

(b) Properties of the effective coefficients ensuring $\mathcal{E}_{\rm n}\geq 0$

From (2.5), the energy $\mathcal{E}_{\rm n}$ supported by the interface is positive if the coefficient $\mathcal{B}$ and $\mathcal{C}$ are positive (the parameter $\varphi_{\rm n}e$ is obviously positive) and this is what we shall prove now.

(i) Bound on $\mathcal{C}$

The parameter $\mathcal{C}$ is defined by $\mathcal{C}=\int_{\mathcal{Y}^-}{\rm d}\boldsymbol{y}\,\partial Q_2/\partial y_2=\int_{\mathcal{Y}^-}{\rm d}\boldsymbol{y}\,\partial Q_3/\partial y_3$ and we use the problem on Q_2 in (3.32). It is sufficient to remark that

$$0=\int_{\mathcal{Y}}{\rm d}\boldsymbol{y}\,(Q_2-y_2)\Delta Q_2=-\int_{\mathcal{Y}^-}{\rm d}\boldsymbol{y}\,|\boldsymbol{\nabla}Q_2|^2+\int_{\mathcal{Y}^-}{\rm d}\boldsymbol{y}\,\frac{\partial Q_2}{\partial y_2}-\int_{\mathcal{Y}^+}{\rm d}\boldsymbol{y}\,|\boldsymbol{\nabla}Q-\boldsymbol{e}_2|^2, \tag{4.4}$$

to get that $\mathcal{C}\geq 0$. In the above integration by parts, the boundary term $\int_{\partial\mathcal{Y}}{\rm d}S(Q_2-y_2)\partial_n Q_2$ vanishes since (i) on the rigid parts of $\mathcal{Y}$, $\partial_n Q_2=0$, (ii) in the connected regions, (Q_2-y_2) and $\boldsymbol{\nabla}Q_2$ are periodic, and (iii) at $y_1\to\pm\infty$, $\partial_n Q_2=\boldsymbol{\nabla}Q_2\cdot\boldsymbol{e}_1=0$. Also, we have used that

$$\int_{\mathcal{Y}^+}{\rm d}\boldsymbol{y}\,\boldsymbol{\nabla}(Q_2-y_2)\boldsymbol{\nabla}Q_2=\int_{\mathcal{Y}^+}{\rm d}\boldsymbol{y}\,|\boldsymbol{\nabla}Q_2-\boldsymbol{e}_2|^2+\int_{\mathcal{Y}^+}{\rm d}\boldsymbol{y}\,\frac{\partial(Q_2-y_2)}{\partial y_2}, \tag{4.5}$$

and the last integral of the right hand-side term vanishes since (Q_2-y_2) is periodic in $\mathcal{Y}^+$.

(ii) Bound on $\mathcal{B}$

It is more demanding to show that $\mathcal{B}\geq 0$. We shall use that the solution Q_1 of the elementary problem (3.32) admits an equivalent variational formulation. If we introduce Q_1^a the solution of

$$\Delta Q_1^a=0\ \text{in}\ \mathcal{Y},\quad \partial_n Q_{1|\Gamma}^a=0,\quad \frac{\partial Q_1^a}{\partial y_1}=\frac{1}{\varphi_{\rm c}}\ \text{at}\ y_1=-y_1^m,\quad \frac{\partial Q_1^a}{\partial y_1}=1\ \text{at}\ y_1=y_1^m, \tag{4.6}$$

then Q_1 solution of (3.32) is the limit of Q_1^a when $y_1^m \to \infty$. Next, Q_1^a minimizes the energy functional

$$\begin{cases} E(Q_1^a) \le E(\tilde{Q}), \\ E(\tilde{Q}) = \displaystyle\int_{\mathcal{Y}} \mathrm{d}\boldsymbol{y}\, \frac{1}{2}|\nabla \tilde{Q}|^2 - D(\tilde{Q}), \end{cases} \tag{4.7}$$

where

$$D(\tilde{Q}) = \int_{\mathsf{Y}} \mathrm{d}\boldsymbol{y}'\, \tilde{Q}(\boldsymbol{x}', y_1^m, \boldsymbol{y}', t) - \frac{1}{\varphi_c} \int_{\mathsf{Y}_a} \mathrm{d}\boldsymbol{y}'\, \tilde{Q}(\boldsymbol{x}', -y_1^m, \boldsymbol{y}', t), \tag{4.8}$$

for any test function $\tilde{Q}$ with a gradient being square integrable (in fact $\tilde{Q}$ in $\mathrm{H}^1(\mathcal{Y})$) and periodic on $\mathcal{Y}^+$ (see additional remark in the Supplementary material). Now, it is easy to see that

$$E(Q_1^a) = -\frac{D(Q_1^a)}{2}. \tag{4.9}$$

To get the above result, we have used that $0 = \int_{\mathcal{Y}} \mathrm{d}\boldsymbol{y}\, Q_1^a \Delta Q_1^a = -2E(Q_1^a) - D(Q_1^a)$. We now choose a test function $\tilde{Q}$ depending on y_1 only and of the form

$$\tilde{Q}(\boldsymbol{y}) = \begin{cases} \dfrac{y_1 + e}{\varphi_c}, & y_1 < -e, \\ \alpha(y_1 + e), & -e < y_1 < 0, \\ \alpha e + y_1, & y_1 > 0, \end{cases} \tag{4.10}$$

and at this stage, α is a free parameter. The energy $E(\tilde{Q})$ in (4.7) is $E(\tilde{Q}) = e\left[\varphi_{\mathrm{n}}\alpha^2/2 - \alpha\right] - y_1^m/2 - y_1^m/(2\varphi_c) + e/(2\varphi_c)$, and it is minimum for $\alpha = 1/\varphi_{\mathrm{n}}$, resulting in

$$E(\tilde{Q}) = \frac{e}{2}\left(\frac{1}{\varphi_{\mathrm{c}}} - \frac{1}{\varphi_{\mathrm{n}}}\right) - \frac{y_1^m}{2} - \frac{y_1^m}{2\varphi_c}. \tag{4.11}$$

It is now sufficient to plug (4.9) and (4.11) in the inequality (4.7) to get

$$D(Q_1^a) \ge e\left(\frac{1}{\varphi_{\mathrm{n}}} - \frac{1}{\varphi_{\mathrm{c}}}\right) + y_1^m + \frac{y_1^m}{\varphi_c}. \tag{4.12}$$

Finally, using Eq. (3.33), we have for $y_1^m \to \infty$: $D(Q_1^a) \sim B_1^+ + y_1^m - \left(B_1^- - y_1^m/\varphi_c\right)$, whence

$$\mathcal{B}_1 \ge e\left(\frac{1}{\varphi_{\mathrm{n}}} - \frac{1}{\varphi_{\mathrm{c}}}\right). \tag{4.13}$$

With our choice of $\tilde{Q}$, we do not get a bound which guaranties $\mathcal{B}_1 > 0$. However, once the enlarged version of the interface is considered, with $\mathcal{B} = \mathcal{B}_1 + e/\varphi_{\mathrm{c}}$ in (2.2) (see (3.52)-(3.53)), we have

$$\mathcal{B} \ge \frac{e}{\varphi_{\mathrm{n}}}. \tag{4.14}$$

The above inequality shows that $\mathcal{B}$ is positive for any relative opening of the neck $0 < \varphi_{\mathrm{n}} \le 1$.

5. Concluding remarks

We have proposed a modeling of an array of resonators of the Helmholtz type. In the effective problem, the region of the cavities is replaced by an anisotropic homogeneous medium which is simply related to the sectional area of the cavities and the region of the necks is replaced by jump conditions. These jumps involved effective parameters given by static problems corresponding to problems of potential flows. In general, these problems have to be solved numerically but their resolution is not very demanding (for instance, they admit a simple variational formulation). Beside, they can be solved once and for all, in a preprocessing step, since they are time independent.

Next, because the problem is written in the time domain, the equation of the energy conservation can be considered, which involves a flux of the Poynting vector associated to the homogenized interface. We have shown that this flux can be rewritten as the time derivative of a positive definite energy; this ensures that the homogenized problem is written in a

suitable form for the numerical implementation in the time domain. Remarks on this numerical implementation can be made. The effective problem is significantly simpler than the actual one since the subwavelength structuration has disappeared; whence, the mesh grid is simply conditioned by the typical wavelength imposed by the source. However, this does not mean that the implementation is straightforward, since it requires the jump conditions to be properly accounted for; an example of such implementation has been proposed in [18]. This problem does not arise for simple scattering problems, and the example of an incident plane wave in the harmonic regime is presented in the Supplementary Material of this paper (an explicit solution of the homogenized problem is available in this case), see also the Appendix.

An interesting extension of the present study concerns the case where the cavities are disjointed, that is when there is air between two successive cavities. In this case, the elementary cell $\mathcal{Y}$ contains two disconnected regions of air, inside and outside the cavity. This leads to the appearance of two elementary problems Q_1^a and Q_1^b instead of the single problem Q_1 in (3.32), with Q_1^a corresponding to the problem of a perfect fluid flowing along $\mathbf{e}_1$ in both regions and Q_1^b corresponding to the problem of a perfect fluid flowing with opposite directions in the two regions.

Data accessibility statement. This work does not have any external supporting data.

Competing interests statement. We have no competing interests

Authors' contributions. All the authors have participated in the reflection on the problem, set up the formalism and they have written the paper.

Funding. The authors acknowledge the financial support of the french Mission Interdisciplainare du Centre National de la Recherche Scientifique (MI/CNRS) under grant INFYNITI/PomS.

A. From a slot to a Helmholtz resonator

In this appendix, we illustrate the robustness of the effective problem, namely its ability to describe the shift in the resonance frequency from that of a slot resonator (in the limit problem) to that of a Helmholtz resonator when h is increased. To do so, we consider an incident wave $e^{ikx-i\omega t}$ on a two-dimensional array with a simple geometry (we shall omit the time dependance in the following). The solution of the effective problem reads as

$$\begin{cases} p(x_1) = e^{ikx_1} + Re^{ikx_1}, & x_1 > 0 \\ p(x_1) = A\cos(k(x_1+d)), & -d < x_1 < 0. \end{cases} \tag{A 1}$$

Finally, for simplicity, we just consider the jump in the pressure in (2.2), with $[\![u]\!] = 0$ (the solution of the full problem is provided in the Supplementary material). Then, (A, R) read as

$$\begin{cases} R = \dfrac{\cot kd - B\varphi_c kh + i\varphi_c}{\cot kd - B\varphi_c kh - i\varphi_c}. \\ A = \dfrac{2/\sin kd}{\cot kd - B\varphi_c kh - i\varphi_c}, \end{cases} \tag{A 2}$$

which remains finite at any frequency. Next, the Helmholtz resonance corresponds to

$$\cot k_R d = B\varphi_c k_R h. \tag{A 3}$$

The limit problem is obtained for $h = 0$, resulting in the quarter wavelength resonance $\cot k_R d = 0$. The order 2 captures the shift with respect to this situation with an increasing impact when increasing h, as expected. This is illustrated in the Fig. 8. We reported the variations of R against

kd for $h = 0.01$, 0.1 and 1 (otherwise, $d = 4$ is fixed and $e/h = 0.5$, $\varphi = 0.5$ and $\varphi_n = 0.01$). It

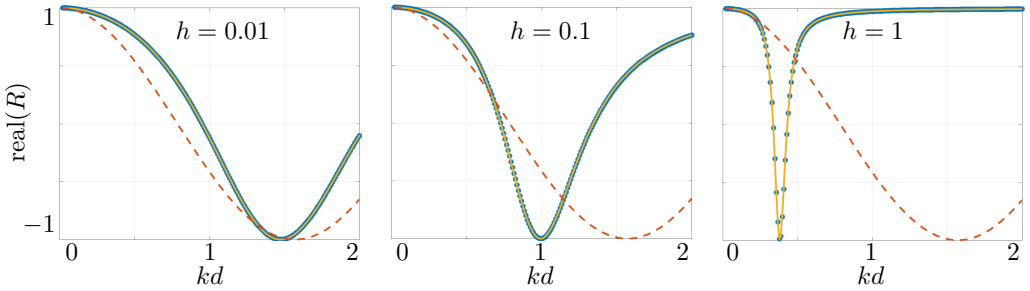

Figure 8. Variations of the real part of R as a function of kd for decreasing h. Open symbols correspond to the direct numerics, plain lines Eq. (A 2) with $B = 52.3$ given by the resolution of the elementary problem. Dotted lines show R at the leading order ($h = 0$ in Eq. (A 2)).

appears that the model is unexpectedly robust with a second order correction able to account for a significant decrease in the resonance frequency. Accordingly, the fields in the model at the order 2 becomes conform to the traditional description of the Helmholtz resonance: with the decrease in the resonance frequency, the field in the cavity, (A 2), becomes almost uniform with an increasing amplitude. This is illustrated in Figs. 9 and 10. We reported the pressure field calculated numerically and in the effective problem (the same for the profile of $|p(x_1, 0)|$ in a single cavity), from (A 2). Further comparisons can be found in the Supplementary material.

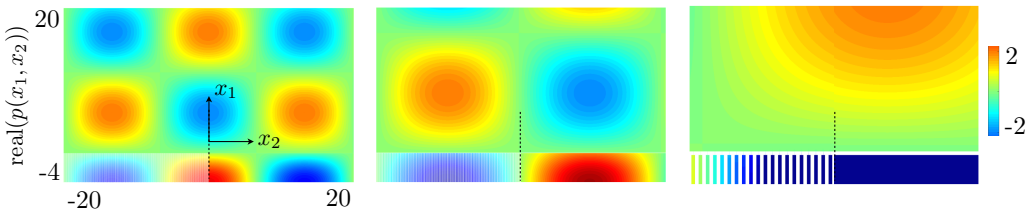

Figure 9. Real part of p at the Helmholtz resonance for $h = 0.01$, 0.1 and 1 (same configuration as in Fig. 8, with an incidence angle of $40°$). In each case, the left part $x_2 < 0$ of the figure show the homogenized solution (up to order 1) and the right part $x_2 > 0$ shows the field calculated numerically. The array of resonators occupies the region $x_1 < 0$.

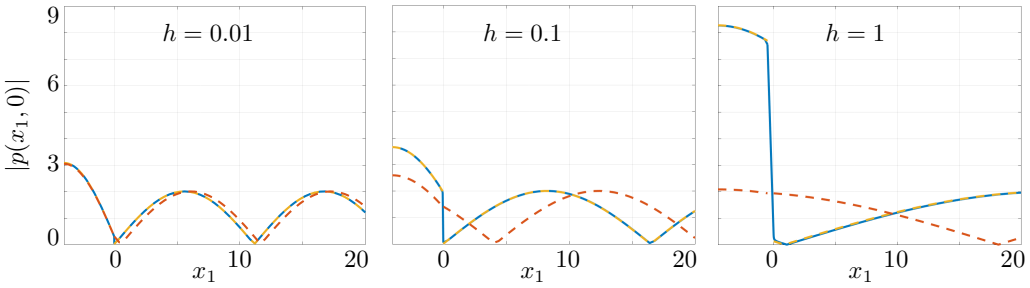

Figure 10. Profiles $|p(x_1, 0)$ across a single resonator (from 9), with the numerical solution in blue plain line, the homogenized solution up to the order 1 in dotted yellow lines and the homogenized solution at the order 0 in dotted red lines.

References

1. Helmholtz HL. 1954 On the Sensations of Tone as a Physiological Basis for the Theory of Music. A.J. Ellis (Ed. and trans.) New York: Dover, (Original German publication, 1863).
2. Valière JC, Palazzo-Bertholon B, Polack JD, Carvalho P. 2013 Acoustic Pots in Ancient and Medieval buildings: Literary analysis of ancient texts and comparison with recent observations in French churches. *Acta Acustica united with Acustica* **99**(1), 70-81.
3. Xiong L, Bi W, Aurégan Y. 2016 Fano resonance scatterings in waveguides with impedance boundary conditions. *J. Acoust. Soc. Am.* **139**(2), 764-772.
4. Romero-García V, Theocharis G, Richoux O, Merkel A, Tournat V, Pagneux V. 2016 Perfect and broadband acoustic absorption by critically coupled sub-wavelength resonators. *Sc. Reports* **6**.
5. Jiménez N, Huang W, Romero-García V, Pagneux V, Groby JP. 2016 Ultra-thin metamaterial for perfect and quasi-omnidirectional sound absorption. *Appl. Phys. Lett.* **109**, 121902.
6. Yang X, Yin J, Yu G, Peng L, Wang N. 2015 Acoustic superlens using Helmholtz-resonator-based metamaterials. *App. Phys. Lett.* **107**(19), 193505.
7. Lemoult F, Fink M, Lerosey G. 2011 Acoustic Resonators for Far-Field Control of Sound on a Subwavelength Scale. *Phys. Rev. Lett.* **107** 064301.
8. Lerosey G, De Rosny J, Tourin A, Fink A. 2007 Focusing beyond the diffraction limit with far-field time reversal. *Science*, **315**(5815), 1120-1122.
9. Maznev AA, Gu G, Sun SY, Xu J, Shen Y, Fang N, Zhang SY. 2015 Extraordinary focusing of sound above a soda can array without time reversal. *New J. Phys.* **17**(4), 042001.
10. Ingard U. 1953 On the theory and design of acoustic resonators. *J. Acoust. Soc. Am.* **25**(6), 1037-1061.
11. Kergomard J, Garcia A. 1987 Simple discontinuities in acoustic waveguides at low frequencies: critical analysis and formulae. *J. Sound Vib.* **114**(3), 465-479.
12. Schwan L, Umnova O, Boutin C. 2017, Sound absorption and reflection from a resonant metasurface: Homogenisation model with experimental validation. *Wave Motion* **72** 154-172.
13. Schweizer, B. 2014 The low-frequency spectrum of small Helmholtz resonators. *Proc. R. Soc. A* **471**(2174) 20140339.
14. Schweizer, B. 2017 Resonance Meets Homogenization. *Jahresbericht der Deutschen Mathematiker-Vereinigung*, **119**(1), 31-51.
15. Lamacz, A, Schweizer B. 2016 Effective acoustic properties of a meta-material consisting of small Helmholtz resonators. arXiv preprint arXiv:1603.05395.
16. Pham K, Maurel A, Marigo JJ. 2017 Two scale homogenization of a row of locally resonant inclusions-the case of anti-plane shear waves. *J. Mech. Phys. of Solids* **106**, 80-94.
17. Felbacq D, Bouchitté G. 2005 Theory of mesoscopic magnetism in photonic crystals. *Phys. Rev. Lett.* **94**(18), 183902.
18. Lombard B, Maurel A, Marigo JJ. 2017 Numerical modeling of the acoustic wave propagation across an homogenized rigid microstructure in the time domain. *J. Comp. Phys.* **335** 558-577.
19. Marigo JJ, Maurel A. 2017 Second Order Homogenization of Subwavelength Stratified Media Including Finite Size Effect. *SIAM J. Appl. Math.* **77**(2), 721-743.
20. Delourme B. 2010 Modèles et asymptotiques des interfaces fines et périodiques en électromagnétisme (Doctoral dissertation, Université Pierre et Marie Curie-Paris VI).
21. Marigo JJ, Maurel A. 2016 Homogenization models for thin rigid structured surfaces and films. *J. Acoust. Soc. Am.* **140**, 260-273.
22. Marigo JJ, Maurel A, Pham K, Sbitti S. 2017 Effective dynamic properties of a row of elastic inclusions: the case of scalar shear waves. *J. Elast.* **128**(2), 265-289.
23. Jiménez N, Romero-García V, Pagneux V, Groby JP. 2016 Quasi-perfect absorption by sub-wavelength acoustic panels in transmission using accumulation of resonances due to slow sound. *Phys. Rev. B* **95**, 014205.
24. Bakhvalov NS, Panasenko G. 2012 Homogenisation: averaging processes in periodic media: mathematical problems in the mechanics of composite materials (Vol. 36). Springer Science & Business Media.
25. Marigo JJ, Pideri C. 2011 The effective behavior of elastic bodies containing microcracks or microholes localized on a surface. *International Journal of Damage Mechanics* **20**(8), 1151-1177.
26. Hewett DP, Hewitt IJ. 2016 Homogenized boundary conditions and resonance effects in Faraday cages. *Proc. R. Soc. A* **472**(2189) 20160062.
27. Maurel A, Marigo JJ, Ourir A. 2016 Homogenization of ultrathin metallo-dielectric structures leading to transmission conditions at an equivalent interface. *J. Opt. Soc. Am. B* **33**(5), 947-956.

28. Mercier JF, Cordero ML, Félix S, Ourir A, Maurel A. 2015 Classical homogenization to analyse the dispersion relations of spoof plasmons with geometrical and compositional effects. *Proc. R. Soc. A* **471**, 20150472.
29. Marigo JJ, Maurel A. 2017 An Interface Model for Homogenization of Acoustic Metafilms. in Handbook of Metamaterials Properties, Vol 2, (Eds.) R V Craster and S Guenneau, World Scientific Publishing Company (2017).
30. Delourme B, Haddar H, Joly P. 2012 Approximate models for wave propagation across thin periodic interfaces. *J. Mathématiques pures et appliquées* **98**, 28-71.